ISSN 1392-1207. MECHANIKA. Vol. 32, No. 3, 2026: 241–250

Process Optimization of Ultrasonic Vibration-Assisted Electrical Discharge Machining for Brass Nozzles Based on Orthogonal Experiments and IPSO-BP Model

Lu CHEN*, Haishan LIAN, Yue LING**, Shanshan YOU**, Deyun MO**, Lingpeng ZHANG**, Guangbin WANG****

**School of Physical Science and Technology, Lingnan Normal University, Zhanjiang, China*

***School of Mechanical and Electrical Engineering, Lingnan Normal University, Zhanjiang, China,*

E-mail: lianhs@lingnan.edu.cn (Corresponding Author: Haishan LIAN)

https://doi.org/10.5755/j02.mech.44449

1. Introduction

Electrical discharge machining is a subtractive manufacturing process for conductive materials based on electrothermal effects. During machining, controlled repetitive electrical discharges are employed, which effectively avoid the stress and vibration problems associated with conventional mechanical turning. Accordingly, EDM is an ideal machining method for array-type fluid and gas guiding holes [1-2]. However, as debris accumulates during the EDM process, the pulse discharge at different positions of the electrode is adversely affected, leading to a reduction in MRR and an increase EWR. Introducing ultrasonic vibrational motion to the tool can effectively enhance debris evacuation [3-4]. The mechanism is utilizing the pumping effect of ultrasonic vibration to gradually expel eroded particles from the discharge gap, thereby improving debris removal and deionization capability, consequently achieving significant enhancements in machining accuracy and efficiency [5-6].

Ultrasonic vibration assisted EDM dependence on various process parameters to meet several diverse and conflicting goals. Common controllable process parameters include machining voltage, pulse frequency, peak current, electrode feed rate, and duty cycle, among others. Meanwhile, performance measurements include MRR, EWR, and surface roughness (SR). Numerical and empirical models are crucial methods for revealing the non-linear mechanisms by which process parameters influence EDM performance across varying application scenarios. Gao et al. [7] optimize the ultrasonic vibration-assisted EDM of SiCp/Al composites using flow field simulation and orthogonal experiments combined with gray relational analysis. Xu et al. [8] and Dinh et al. [9] employ Plackett-Burman or Box-Behnken designs to develop second-order models for multi-objective optimization, demonstrating that refined settings enhance machining performance in applications such as micro holes with large depth to diameter ratios by facilitating debris evacuation and discharge stability. Jatti et al. [10] develop a 3D finite element model to simulate the single discharge process and predict the material removal rate based on temperature profiles, validating the model's accuracy with an average error of approximately 6.2%. Arif et al. [11] developed a modified Gaussian heat flux model and conducted finite element simulations to investigate the effects of different tool materials in EDM. The outcomes indicated that higher tool electrical conductivity increases work piece residual stress, while MRR and SR rise with key electrical parameters. In addition to regression and numerical models, experimental methods have also been widely employed to optimize EDM process parameters. [12-15]. Perumal et al. [16] employed the Taguchi orthogonal array and Grey Relational Analysis to optimize EDM parameters such as discharge current, spark on time and tool diameter for machining a high-strength titanium alloy, finding that spark on time is the most influential parameter on machining characteristics. Pratap et al. [17] applied Grey Relational Analysis and Weighted Principal Component Analysis to optimize EDM parameters for Inconel X-750, determining that the parameter combination of 15A peak current, 74μs pulse on time, 8μs pulse off time, and 40V voltage yielded the best comprehensive performance in terms of MRR and SR.

The aforementioned methods are capable of identifying relatively optimal combinations of process parameters to a certain extent. However, in most of these approaches, the parameter levels are arranged in a hierarchical and incremental manner, or the regression equations employed fail to comprehensively capture the complex relationships among multiple factors. Therefore, based on the experimental data already obtained, training a targeted artificial neural network (ANN) model for the specific machining conditions can provide more reliable predictive guidance for the subsequent adjustment and optimization of process parameters [18-21]. Akar et al. [22] employed a hybrid ANN/PSO technique to model and optimize the μwire-EDM process of a NiTi super alloy, and found that a comprehensive optimization strategy involving the combined adjustment of pulse on time, pulse off time, discharge current, and servo voltage effectively minimized kerf width and SR while maintaining the white layer thickness. Dilip et al. [23] propose a hybrid approach combining response surface methodology and a genetic algorithm to determine the optimal cutting conditions, which successfully reduces the inner sidewall surface roughness to 1.3587 μm. The predicted responses are subsequently validated through experiments, with the maximum relative error being less than 10%, similar work is also reported by Dutta et al. [24]. Zhang et al. [25] establish a BP neural network model based on orthogonal experiments to predict machining performance in micro-EDM, and the results show that compared to fitted regression equations, the ANN model reduces relative error rates for machining time, axial wear, and radial wear by 77.42%, 78.51%, and 75.92%, respectively. Danish et al.

[26] add carbon nanotubes to the dielectric in EDM of 316L steel and employ the multi-objective ant lion optimizer for parametric optimization, finding that current intensity is the most significant factor and that the model predicted solution sets achieve high predictive accuracy with errors below 10%.

Although combining process parameters with ANN to optimize EDM performance has proven effective, most existing studies rely on standard commercial equipment and generic algorithms, which often lack the targeted accuracy and adaptability required for specific industrial production. In this manuscript, a self-developed multifunctional micro-EDM machine tool serves as the foundational platform, which significantly enhances the flexibility of parameter setting and adjustment during the experiments. Using brass for precision agricultural nozzles as the workpiece material and selecting MRR and EWR as the evaluation indicators, orthogonal experiments are conducted to comprehensively optimize the process parameters of ultrasonic vibration-assisted EDM based on dielectric fluid vibration. Meanwhile, leveraging the capability of BP neural networks to handle multi-factor, multi-condition, and fuzzy information, the orthogonal experimental data is fully utilized for model training and verification. An IPSO algorithm is employed to optimize the hyperparameters of the BP network. In summary, since the inevitable electrode wear during the EDM process significantly impacts the quality and machining efficiency of the micro-cavities in brass nozzles, this study proposes a comprehensive framework integrating customized machine structure, machining solutions, process optimization, and prediction model construction to address this issue. We expect this framework can provide a robust reference for similar micro-machining research.

2. Experimental Details

2.1. Machining device and materials

The experiments are performed on an independently developed multifunctional micro-EDM machine tool. The X and Y axes of this machining device utilize nanometric micro-positioning stages with a resolution of ≤ 0.1 nm, while the Z-axis resolution is ≤ 5 nm. The ultrasonic vibration worktable features a maximum vibration frequency of 40 kHz with adjustable power. The high-frequency pulse EDM power supply offers a continuously adjustable duty cycle ranging from 10% to 90%, along with an output voltage of 0-120 V, a frequency of 1 kHz-100 kHz, and a current of 0-5 A. An expandable pressure sensor is installed between the positioning stage and the ultrasonic vibration liquid tank. The Z-axis is equipped with an NSK electric spindle with a speed range of 1000-80000 rpm. A tungsten carbide electrode is mounted on the electric spindle, rotating and feeding along with the spindle during the machining process [27]. During operation, the motion control module first positions the tool electrode and workpiece rapidly to the initial machining zone. Subsequently, under the synergistic action of the ultrasonic vibration tank and the pulse power supply, the industrial computer adaptively adjusts the feed rate based on the real-time discharge voltage to maintain a stable sparking state. Meanwhile, the data acquisition system (DAQ) and the pressure sensor record signal variations in real time, providing data support for subsequent process optimization, as shown in Fig. 1.

Brass is frequently utilized as the material for precision agricultural spray nozzles due to its corrosion resistance and superior wear resistance compared to plastics. The properties of the brass material machined in this study are presented in Table 1.

Tungsten carbide exhibits low electrical resistivity, enabling it to withstand high-frequency discharges without generating significant resistive heat. Its melting point is significantly higher than that of brass, and its high elastic modulus ensures that no deformation occurs during high-speed rotation and vibration. Furthermore, the fine grain size of tungsten carbide results in uniform electrode wear following discharge, which contributes to improving the quality of the machined surface. The properties of the tungsten carbide electrode material selected for this study are presented in Table 2.

During short pulse discharges, electrons bombard the anode at high velocities, generating immense localized heat. Therefore, tungsten carbide electrode is connected to the cathode, where heat generation is relatively lower. This

Table 1

Material properties of brass

Melting point	~1083℃
Density	8.6×10^{-6} kg/mm^3
Elastic modulus	106 GPa
Poisson's ratio	0.32
Electrical Resistivity	1.7×10^{-5} Ω·mm

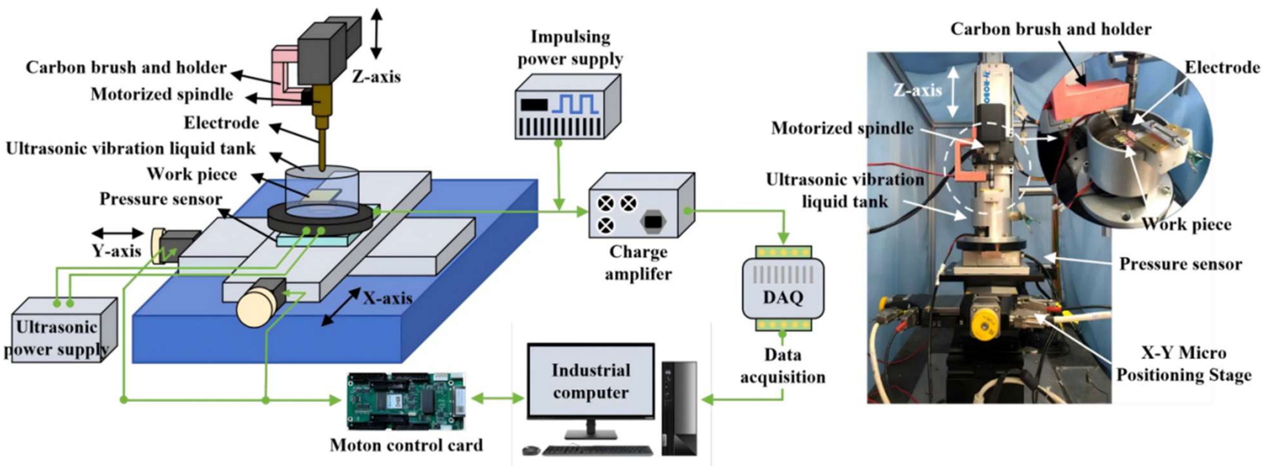

Fig. 1 Ultrasonic vibration-assisted electrical discharge machining system

Table 2
Material properties of electrode

Melting point	~2870℃
Density	15.7×10^{-6} kg/mm^3
Elastic modulus	620 GPa
Poisson's ratio	0.21
Electrical Resistivity	$1.8\times10^{-4}\Omega\cdot$mm

configuration helps reduce the EWR and ensures machining precision. Conversely, the brass workpiece, which has a lower melting point, is connected to the anode, facilitating its melting under electron bombardment to maximize the MRR. During the machining process, the liquid tank is connected to an ultrasonic power supply (maximum output power: 150 W). The ultrasonic vibration induces cavitation and pumping effects in the dielectric fluid, which significantly enhance fluid circulation and debris flushing. However, excessive ultrasonic power leads to continuous heat generation and accelerated equipment wear. Therefore, it is essential to balance the debris removal efficiency with the operational stability of the system by selecting an optimal ultrasonic power level.

2.2. IPSO-BP neural network

The BP (Back Propagation) network is a multi-layer feed forward neural network trained via the error back propagation algorithm, characterized by its powerful adaptive learning and non-linear mapping capabilities. In this study, the BP neural network serves as the core framework for constructing a process prediction model for ultrasonic vibration-assisted EDM. The input layer consists of five neurons, corresponding to machining voltage, pulse frequency, spindle speed, ultrasonic power, and electrode feed rate. The output layer comprises two neurons, representing MRR and EWR. To better capture the non-linear relationship between the inputs and outputs, a BP neural network with double hidden layers is employed, and its structural topology is shown in Fig. 2.

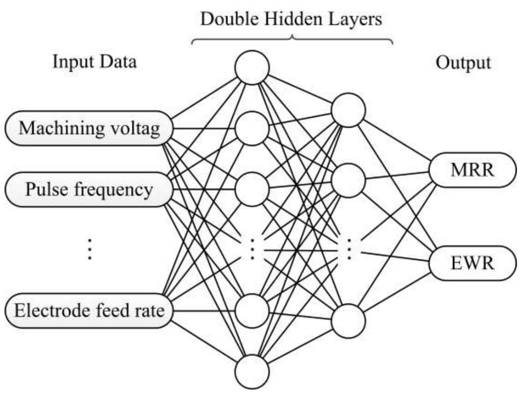

Fig. 2 Topology diagram of BP network

After the topology structure of the BP network is established, the configuration of its hyperparameters significantly influences both the efficiency of the training process and the final outputs. Consequently, employing an optimization algorithm can provide effective guidance for the hyperparameters configuration. PSO is an evolutionary computation algorithm based on the fundamental concept of seeking the optimal solution through collaboration and information sharing among individuals within a population. Through the iteration of position (P_i) and velocity (V_i) in a multi-dimensional space, each search particle continuously evolves towards its individual optimal fitness (F_i) and the global optimal position (G) [28]. The update equations are expressed as follows:

$$V_i^{n+1} = wV_i^n + c_1r_1\left(F_i^n - P_i^n\right) + c_2r_2\left(G - P_i^n\right), \quad (1)$$

$$P_i^{n+1} = P_i^n + P_i^{n+1}, \quad (2)$$

where n is iteration count, the constants c_1 and c_2 are learning factors, r_1 and r_2 are independent random variables within the interval (0, 1), and w representing the inertia weight.

To accurately locate the global optimal solution, it is desirable to assign a larger inertia weight (ω) during the initial iteration phase to facilitate global exploration, while gradually reducing ω in the later phase to enhance the probability of convergence [29]. On the other hand, the algorithm maintains a mechanism to challenge the current results; specifically, a certain proportion of "mutated" particles is introduced in each iteration to conduct random global re-exploration. In summary, the PSO algorithm is improved in two aspects [30]:

$$w = w_{initial} - tanh\left(\frac{n}{N_{total}}\right)\left(w_{initial} - w_{final}\right), \quad (3)$$

where N_{total} is the total iteration time, $w_{initial}$ and w_{final} represent the initial and final inertia weight, respectively.

$$K = 0.5\frac{n}{N_{total}} + 0.5, \quad (4)$$

where K is a threshold that gradually increases with n. During each iteration of the PSO, the top K% of particles with the highest fitness are retained for updating, while the remaining $1-K$% particles are randomly redistributed. This mutation mechanism is analogous to that used in genetic algorithms. To verify the effectiveness of these improvements, the convergence capabilities of the IPSO and the standard PSO are compared using a set of benchmark functions, as illustrated in Fig. 3.

It is evident that although the IPSO incorporating the variable inertia weight ω and the adaptive mutation threshold K sacrifices iteration speed, it demonstrates enhanced and more stable search capability and precision, which facilitates the hyperparameter optimization of the BP neural network. In summary, the workflow of the IPSO-BP model is illustrated in the Fig. 4.

2.3. Experimental procedure

Prior to experimentation, the brass workpiece is cleaned on its top and bottom surfaces with alcohol pads and then secured within the dielectric tank using clamps. During machining, the ultrasonic power supply is activated to transmit high-frequency high-voltage pulsed signals to the ultrasonic transducer. This agitates the dielectric fluid within the ultrasonic vibration platform, thereby inducing cavitation

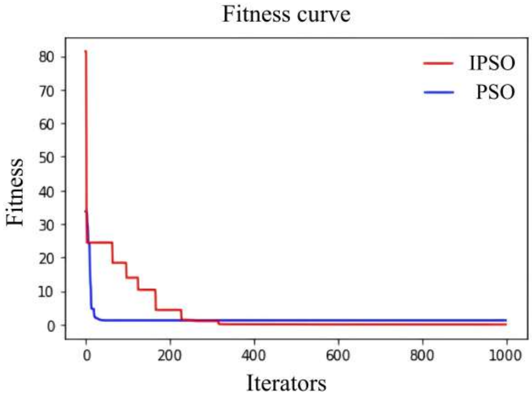

Fig. 3 Convergence performance of IPSO and PSO

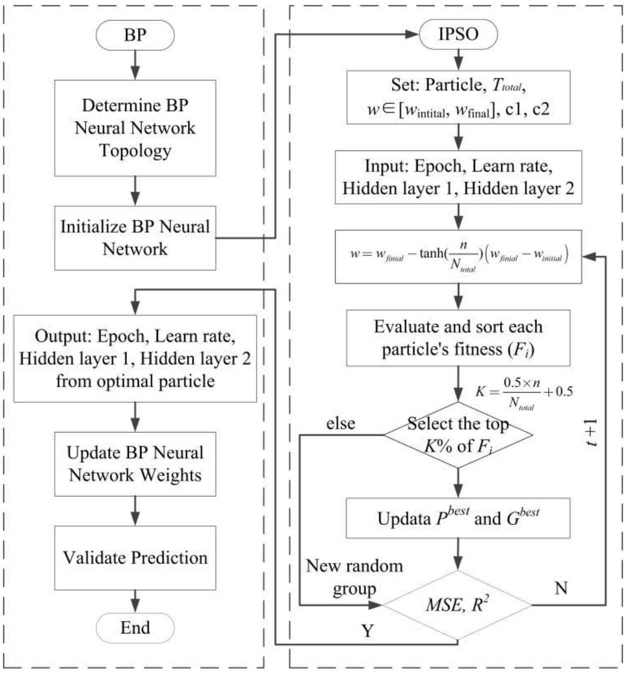

Fig. 4 Workflow of the IPSO-BP model

and pumping effects that accelerate the circulation of the fluid, consequently enhancing the debris evacuation and deionization capabilities of the EDM process. The experimental process parameters are strictly set in accordance with the orthogonal experimental design, and each experimental set is repeated an equal number of times. Upon completion of the experiments, the mass of both the electrode and the workpiece before and after machining is measured using an FA2104J electronic balance with a resolution of 0.1 mg. To ensure data reliability, each measurement is performed three times, and the average value is recorded. Based on these weight measurements, the MRR and EWR are calculated using the following equations:

$$MRR = \frac{m_{m1} - m_{m2}}{\rho_m \times t}, \tag{5}$$

$$EWR = \frac{m_{e1} - m_{e2}}{\rho_e \times t}, \tag{6}$$

where m_{m2} and m_{e2} denote the final weights of the work piece and the electrode, respectively, while m_{m1} and m_{e1} represent their initial weights. The ρ_m and ρ_e is the density of the work piece and electrode, respectively; t is the machining time.

3. Orthogonal Experiment and Results Analysis

The orthogonal experimental design utilizes a brass sheet (46mm ×20 mm × 3mm) as the workpiece, and 1mm diameter tungsten carbide rod, diameter tolerance ±0.01mm as the tool electrode. Deionized water serves as the dielectric fluid using the immersion method. The machining depth is set to 3 mm, and the duty cycle is 50%. Five process parameters are selected: machining voltage, spindle speed, ultrasonic power, pulse frequency, and feed rate. The interactions among these five parameters are not considered. An $L_{16}(4^5)$ orthogonal array is employed for the design, as shown in Table 3. To eliminate random errors and ensure data reliability, each indicator is measured 8 times, and the average value is recorded.

Table 3

Factors and levels of orthogonal experiment.

Levels	A	B	C	D	E
	Machining voltage	Spindle speed	Ultrasonic power	Pulse frequency	Electrode feed rate
1	65	2000	45	25	0.16
2	75	2500	55	30	0.18
3	85	3000	65	35	0.20
4	95	3500	75	40	0.22

3.1. Effect of single-factor variables on machining quality

Before conducting the orthogonal experiments, single-factor experiments are performed to confirm the appropriate selection of factors listed in Table 3. Due to space limitations, two SEM test results for each single-factor variable are selected for comparison, as shown in Fig. 5.

According to the machining quality images in Fig. 5, a and b, the machining quality is superior when the machining voltage is 65V or 95V. However, at 75V and 85V, although the material removal rate increases, significant burrs and edge chipping occur. As shown in Fig. 5, c and d, higher spindle speeds result in better machining quality. Referring to Fig. 5, e and f, the optimal machining performance is achieved when the ultrasonic power is at 55%; either decreasing or increasing the ultrasonic power reduces the machining quality. As shown in Fig. 5, g and h, the quality of the machined holes gradually improves with an increase in pulse frequency. According to Fig. 5, i and j, a higher feed rate leads to lower machining quality.

The single-factor experiments not only demonstrate that the five selected factors influence machining quality, thereby affecting MRR and EWR; but also reveal the specific influence trends of each factor on machining quality. However, single-factor experiments alone are insufficient to reveal the interactive effects among the factors. Therefore, it is necessary to conduct further experiments based on the orthogonal array.

3.2. Orthogonal experiment results and analysis

Origin software is utilized to analyze the real-time voltage, current, and displacement graphs obtained from

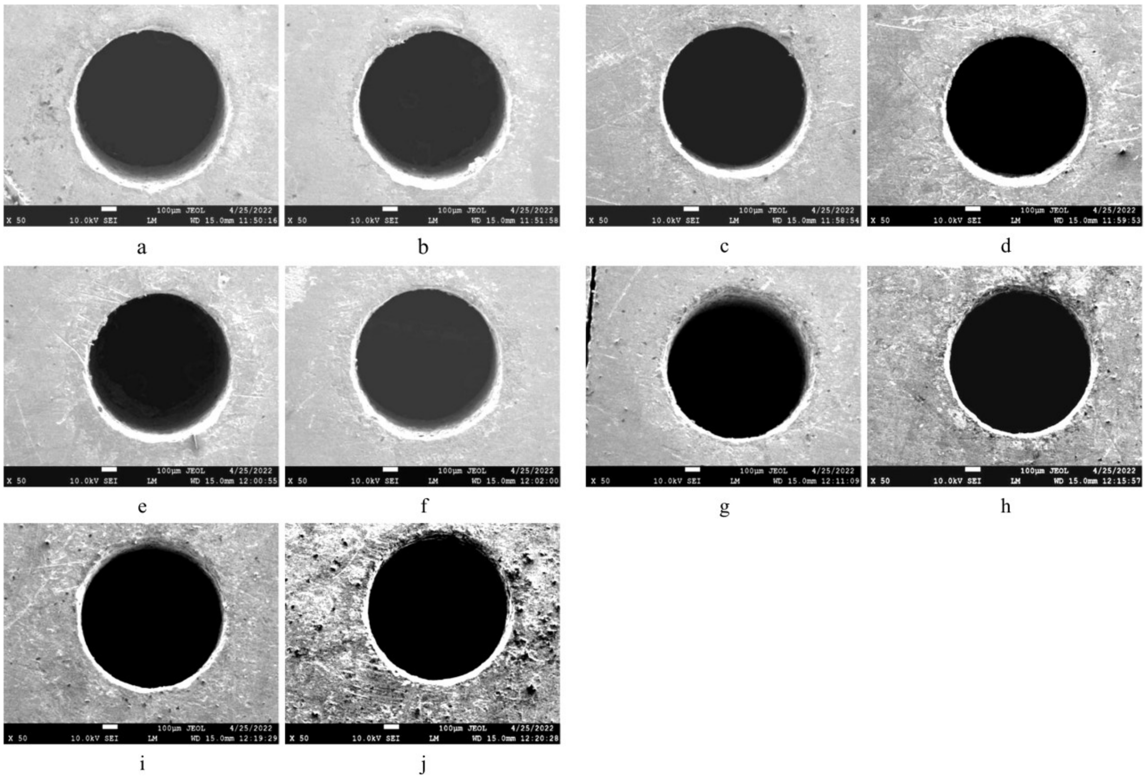

Fig. 5 SEM morphology of the machined hole: a – machining voltage 65 V, b – machining voltage 75 V, c – spindle speed 2000 r/mm, d – spindle speed 2500 r/mm, e – ultrasonic power 45%, f – ultrasonic power 55%, g – pulse frequency 25 kHz, h – pulse frequency 30 kHz, i – electrode feed rate 0.16 mm/s, j – electrode feed rate 0.18 mm/s

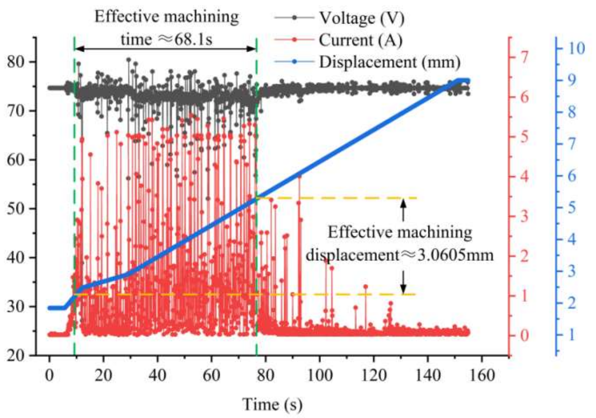

Fig. 6 EDM discharge machining interval

each experimental group. By combining the analyzed data, the discharge machining interval is identified. Within this interval, the difference between the start and end points on the X-axis is defined as the machining time *t*. Taking the EDM data at a machining voltage of 75 V as an example, when the dielectric breaks down and the current surges instantaneously, the current jumps to its peak value. Therefore, the moment of the first sudden change in voltage and current data is set as the machining start point, and the moment when the concentrated discharge ends is set as the machining end point. This is verified using the electrode displacement measurement data (workpiece thickness is 3 mm). Consequently, as shown in Fig. 6, the effective machining time *t* is determined to be approximately 68.1 s, and the effective machining displacement is approximately 3.0605 mm.

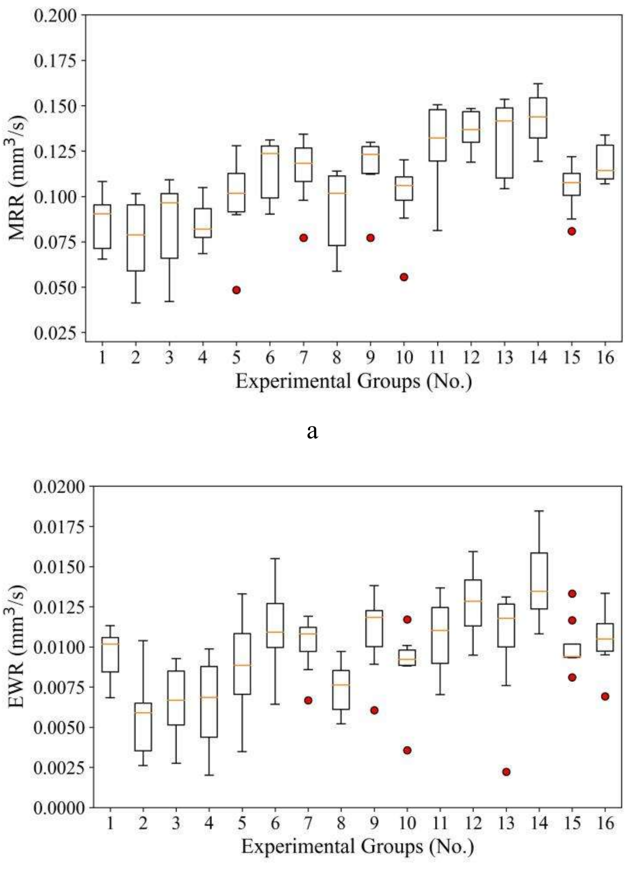

Fig. 7 Statistics of orthogonal experiment data: a – statistics of MRR results, b – statistics of EWR results

The experiments are conducted according to the orthogonal scheme in Table 4, comprising 16 groups of orthogonal experiments. Each group is repeated 8 times. Upon completion of the experiments, the MRR and EWR are recorded. Analysis of the experimental results reveals that even within identical process experiments, data anomalies may still exist. To ensure the reliability of the statistical results, it is necessary to filter out outliers before conducting statistical analysis.

In Fig. 7, 1.5 times the interquartile range (IQR) serves as the criterion for identifying outliers. As indicated by the red dots, there are 5 and 9 outliers in the MRR and EWR experiments, respectively. The outliers account for 14/256 of the total data, approximately 5.4%. To facilitate observation, the MRR and EWR results for each group are scaled up by factors of 10^3 and 10^4, respectively, before being entered into the orthogonal experiment table. The results are presented in Table 4.

Table 4

Orthogonal scheme ($L_{16}(4^5)$)

No.	Factors and Levels					Result, mm^3/s	
	A	B	C	D	E	MRR($\times 10^3$)	EWR($\times 10^4$)
1	1(65 V)	1(2000 r/min)	1 (45%)	1(25 kHZ)	1(0.16 mm/s)	88	94
2	1	2(2500 r/min)	2(55%)	2(30 kHZ)	2(0.18 mm/s)	74	57
3	1	3(3000 r/min)	3(65%)	3(35 kHZ)	3(0.20 mm/s)	83	65
4	1	4(3500 r/min)	4(75%)	4(40 kHZ)	4(0.22 mm/s)	67	62
5	2(75 V)	1	2	3	4	109	92
6	2	2	1	4	3	115	112
7	2	3	4	1	2	114	102
8	2	4	3	2	1	94	76
9	3	1	3	4	2	112	108
10	3(85 V)	2	4	3	1	100	89
11	3	3	1	2	4	128	112
12	3	4	2	1	3	136	133
13	4(95 V)	1	4	2	3	132	115
14	4	2	3	1	4	143	142
15	4	3	2	4	1	106	103
16	4	4	1	3	2	117	114

3.3. Process parameter optimization and verification

Regarding MRR and EWR as the critical indicators, the experimental results are analyzed through range analysis based on the data in Table 4. MRR is a crucial indicator of EDM efficiency; practically, a higher value signifies better performance. The range analysis of MRR is calculated in Table 5.

Table 5 indicates that the order of influence of the process parameters on MRR is A→D→E→C→B. Specifically, the factors ranked from highest to lowest impact are machining voltage, pulse frequency, feed rate, ultrasonic power, and spindle speed. Notably, the weight of the machining voltage is significantly higher than that of the other factors. To corroborate the results of the range analysis, a Pearson's correlation analysis on MRR is further introduced, as shown in Fig. 8.

As depicted in Fig. 8, the significance ranking of the factors affecting MRR is consistent with the range analysis. Machining voltage and electrode feed rate exhibit a positive correlation with MRR, whereas the other three factorsdemonstrate a negative correlation. By combining the results from both methods, it is determined that the optimal process parameter combination for MRR is a machining voltage of 95 V, a spindle speed of 2000 rpm, an ultrasonic power of 45%, a pulse frequency of 25 kHz, and a feed rate of 0.20 mm/s. To further verify the effectiveness of this process combination, this set of parameters is designated as Verification Group 1.

On the other hand, EWR determines production costs; typically, a lower value is desirable in mass production. The range analysis of EWR is calculated in Table 6.

As indicated in Table 6, the order of influence of the process parameters on EWR is A→D→C→E→B. Machining voltage remains the most significant influencing factor, followed by pulse frequency. Similar to that of MRR, a significance analysis on EWR is also introduced, as shown in Fig. 9.

The positive and negative correlation trends of the factors affecting EWR are similar to MRR. The influence weights of feed rate and ultrasonic power are close, while

Table 5

Range analysis of MRR

Indicator MRR	A	B	C	D	E
Avg. 1	78.00	111.25	112.00	120.25	97.00
Avg. 2	108.00	108.00	106.25	107.00	104.25
Avg. 3	119.00	107.75	108.00	102.25	116.50
Avg. 4	124.50	103.50	103.25	100.00	111.75
Range	46.50	6.75	8.75	20.25	19.50
Rank	A→D→E→C→B				
Opt. Process	A4 D1 E3 C1 B1				

Table 6

Range analysis of EWR

Indicator EWR	A	B	C	D	E
Avg. 1	69.50	102.25	108.00	117.75	90.50
Avg. 2	95.50	100.00	96.25	90.00	95.25
Avg. 3	110.50	95.50	97.75	90.00	106.25
Avg. 4	118.50	96.25	92.00	96.25	102.00
Range	49.00	6.75	16.00	27.75	15.75
Rank	A→D→C→E→B				
Opt. Process	A1 D2 C4 E1 B3				

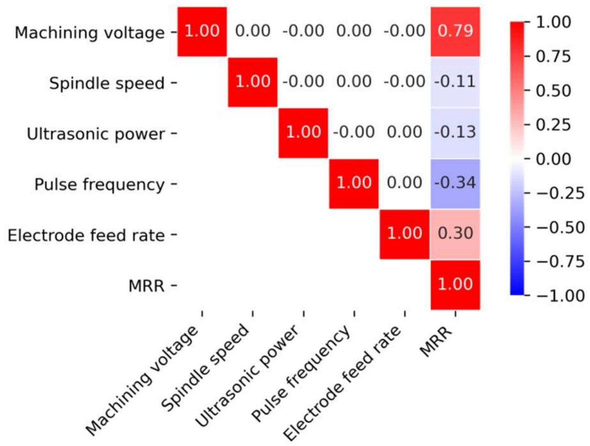

Fig. 8 Pearson's correlation analysis of MRR

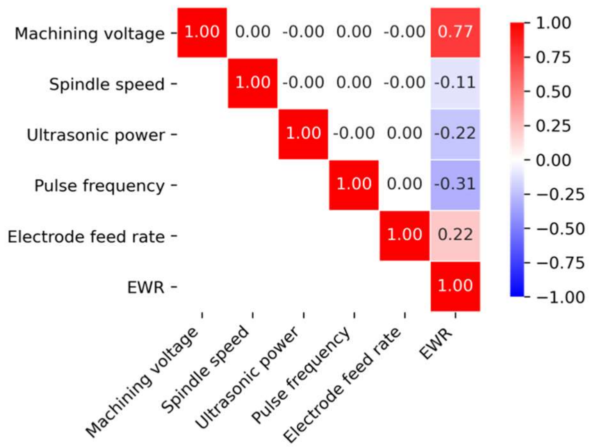

Fig. 9 Pearson's correlation analysis of EWR

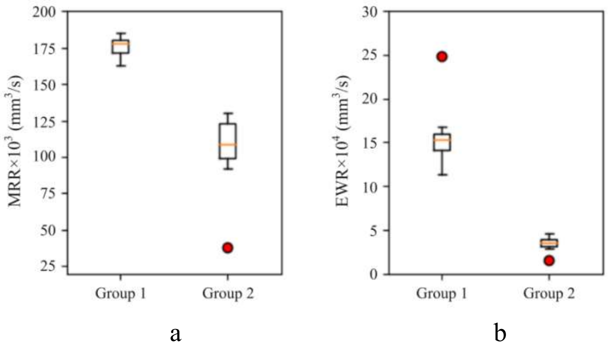

Fig. 10 Statistics of experimental data for the verification group: a – verification group of MRR, b – verification group of EWR

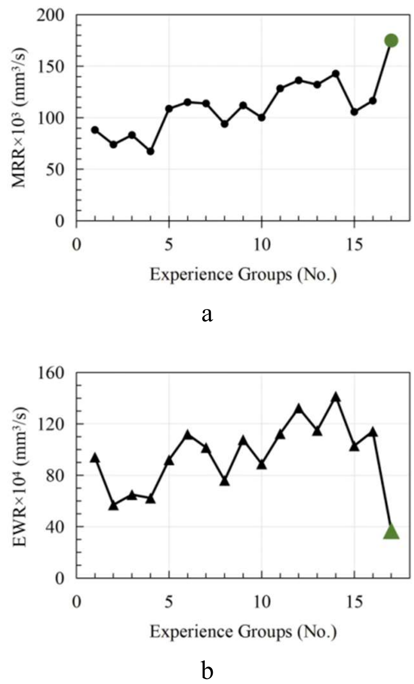

Fig. 11 Comparison of MRR and EWR across experimental groups: a – MRR, b – EWR

the weight of spindle speed is the lowest. Under the premise of ensuring machining quality, a lower pulse frequency helps maintain discharge stability and prevent arcing. Therefore, the optimal process parameter combination for EWR is a machining voltage of 65 V, spindle speed of 3000 r/min, ultrasonic power of 75%, pulse frequency of 30 kHz, and feed rate of 0.16 mm/s. To further verify the effectiveness of this process combination, these parameters are designated as Verification Group 2.

Notably, the pairwise correlation coefficients between the input parameters in Figs. 8 and 9 are 0, confirming the strict orthogonality of the selected L_{16} design. Although this standard array effectively isolates main effects, it does not evaluate parameter interactions. Consequently, the conclusions and optimal combinations derived in this study refer primarily to main factor trends within the tested parameter ranges.

Following the procedure of the orthogonal experiment, experiments for Verification Groups 1 and 2 are each repeated eight times, and the average value is recorded. Consistent with the previous 16 experimental groups, using 1.5 times the IQR as the threshold, outliers in these two groups are detected and removed, as shown in the Fig. 10.

The mean values of the repeated experiments, calculated after outlier removal, are compared with the results of the 16 orthogonal experiment groups, as illustrated in the Fig. 11.

As observed in Fig. 11, the MRR of verification group 1 reaches 176×10^{-3} mm^3/s, surpassing the 143×10^{-3} mm^3/s of experimental group 14. Compared to the 67×10^{-3} mm^3/s of experimental group 4, this represents an improvement of 163%. On the other hand, the EWR of verification group 2 is 37×10^{-4} mm^3/s, which is lower than the 57×10^{-4} mm^3/s of experimental group 2. Compared to the 142×10^{-4} mm^3/s of experimental group 14, this corresponds to a reduction of 74%. This demonstrates that the orthogonal experiment effectively evaluates the influence of various parameters on MRR and EWR, and successfully optimizes the process parameter combinations. Verification group 1 achieves the highest MRR, while verification group 2 achieves the lowest EWR, confirming the success of the verification.

4. IPSO-BP Modeling

Since the orthogonal experiment selects a series of discrete points, the exploration for extrema is hierarchical and discrete. Consequently, when subsequent parameter adjustments are required, additional exploratory experiments may be necessary. To fully utilize the data obtained from the orthogonal experiments, an intelligent prediction model for ultrasonic vibration-assisted EDM is constructed. This model combines the powerful non-linear mapping capability of the BP neural network with the global optimization performance of IPSO, leveraging their proficiency in handling multi-factor coupling and imprecise information. The objective is to accurately evaluate the effects of process parameter adjustments within the range defined by the orthogonal experimental design without the need for supplementary experiments for this specific machining system.

Using Fig. 4 as the primary framework for the IPSO-BP model, the following steps are implemented:

1. From the 16 experimental groups in Table 4, the 254 data points remaining after the removal of outliers serve as the training (80%) and validation (20%) samples for the BP neural network. The data is preprocessed using Z-score normalization, and a fixed random seed is set to ensure repeatability during the hyperparameter optimization process.
2. The optimization targets and ranges for the IPSO are set as follows: BP neural network learning rate ∈ [0.001, 0.01], nodes in hidden layer 1 ∈ [1, 100], nodes in hidden layer

2. ∈ [1, 100], and epoch ∈ [10, 60]. According to Eq. (3), the parameters of the IPSO are configured with $w_{initial} = 0.8$, $w_{min} = 0.5$, $N_{total} = 20$, and a swarm size of 20 particles.

3. The iterative optimization process is repeated until the predicted values for each indicator reach stable convergence, and the model performance is verified using the optimal combination of process parameters.

During training, R^2 (coefficient of determination, dimensionless) and *MSE* (mean squared error, square of the corresponding evaluation index) are used to evaluate the relationship between the predicted values and the actual values. They are expressed as follows:

$$R^2 = 1 - \frac{\sum_{i=1}^{n} (y_i - \hat{y}_i)^2}{\sum_{i=1}^{n} (y_i - \bar{y}_i)^2}, \tag{7}$$

$$\bar{y} = \frac{1}{n} \sum_{i=1}^{n} y_i, \tag{8}$$

$$MSE = \frac{1}{n} \sum_{i=1}^{n} (y_i - \hat{y}_i)^2, \tag{9}$$

where y_i is the actual value, $\hat{y}$ is the predicted value, $\bar{y}$ is the average of the actual value, and the n is the number of samples. A larger R^2 indicates better model performance, while a smaller *MSE* indicates the opposite.

The hybrid model selects ReLU as the activation function; compared to the commonly used sigmoid and tanh functions, ReLU offers better differentiability and enhances the network's non-linear fitting capability. Adam is chosen as the optimizer to improve computational efficiency. The hyperparameters of the BP neural network optimized by IPSO are presented in the Table 7.

The repeated experiments from the orthogonal optimization scheme, following the removal of outliers, serve as the validation set: 15 sets for MRR and 14 sets for EWR. The IPSO-BP is employed to predict these two indicators, as illustrated in the Fig. 12.

As observed in Fig. 12, for the validation of both indicators, the predicted results fall within the fluctuation range of the repeated experiments, effectively capturing the variation trends of the experimental data. Regarding specific

Table 7

The hyperparameters optimized by IPSO

Hyperparameters	Optimization Results
Learning rate	0.0034
Hidden layer 1	79
Hidden layer 2	77
Epoch	16

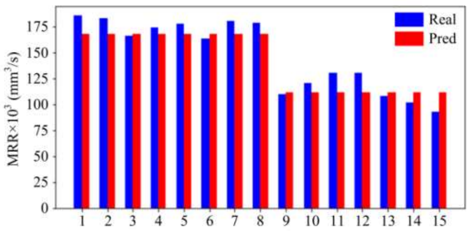

a

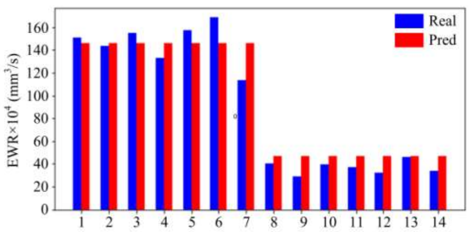

b

Fig. 12 Prediction performance of the IPSO-BP model: a – predicted vs. actual MRR, b – predicted vs. actual EWR

results, for the MRR prediction in Fig. 10(a), the R^2 is 87% and the *MSE* is 152×10^{-3} $(mm^3/s)^2$. For the EWR prediction in Fig. 10, b, the R^2 reaches 94% with an *MSE* of $203\times10^{-4}(mm^3/s)^2$. The overall prediction performance is satisfactory. The reliability demonstrated by the IPSO-BP hybrid model in predicting the ultrasonic vibration-assisted EDM process within the investigated parameter space facilitates future process adjustments for similar brass nozzle machining tasks on specific experimental platform.

5 Conclusions

Based on the combination of five-factor four-level orthogonal experiments and the IPSO-BP model, this paper investigates the parameter optimization for MRR and EWR in ultrasonic vibration-assisted EDM of 3 mm thick brass. The optimal process parameter combinations are determined, and the main conclusions are as follows:

1. According to the orthogonal experiments and range analysis, the order of influence of process parameters on MRR, in descending order, is: machining voltage > pulse frequency > feed rate > ultrasonic power > spindle speed. Similarly, the order of influence on EWR is: machining voltage > pulse frequency > ultrasonic power > feed rate > spindle speed.

2. Through orthogonal experiments combined with Origin image analysis and weight measurement analysis, the optimal process parameter combination for MRR is determined as: machining voltage 95 V, spindle speed 2000 rpm, ultrasonic power 45%, pulse frequency 25 kHz, and feed rate 0.20 mm/s. This process increases the MRR to 176×10^{-3} mm^3/s. The optimal process parameter combination for EWR is: machining voltage 65 V, spindle speed

3000 rpm, ultrasonic power 75%, pulse frequency 30 kHz, and feed rate 0.16 mm/s. This process reduces the EWR to 37×10^{-4} mm^3/s.

3. Through the above analysis and verification, the IPSO-BP hybrid model demonstrates excellent reliability. In tests using the orthogonal experiment optimization scheme as the validation set, the R^2 values for MRR and EWR are 87% and 94%, respectively, while the *MSE* values are 152×10^{-3} $(mm^3/s)^2$ and 203×10^{-4} $(mm^3/s)^2$. This model facilitates savings in material and time during subsequent process adjustments and can be utilized to guide actual industrial production and scientific research practices.

Acknowledgments

The research work was supported by Guangdong Province general university Special projects in key areas (2023ZDZX3011); Zhanjiang non-funded science and technology research project (2024B01087); Lingnan Normal University scientific research project (TL2407, LZ2204); Guangdong Province general university innovation team project (2025KCXTD02).

References

1. **Hasan, M. M.; Saleh, T.; Sophian, A.; Rahman, M. A.; Huang, T.; Ali, M. S. M.** 2023. Experimental modeling techniques in electrical discharge machining (EDM): A review, The International Journal of Advanced Manufacturing Technology 127: 2125-2150. https://doi.org/10.1007/s00170-023-11603-x.
2. **Meshram, D. B.; Puri, Y. M.** 2017. Review of research work in die sinking EDM for machining curved hole, Journal of the Brazilian Society of Mechanical Sciences and Engineering 39(7): 2593-2605. https://doi.org/10.1007/s40430-016-0622-7.
3. **Maher, I.; El-Hofy, H.; El-Hofy M. H.** 2023. Ultrasonic Vibration Assisted Electrical Discharge Machining and Micro-Electrical Discharge Machining: A Review, Machining Science and Technology 27(6): 653-696. https://doi.org/10.1080/10910344.2023.2263780.
4. **Shah, M. S.; Saha, P.** 2021. Assessment of vibration-assisted micro-EDM dressing process-stability by monitoring and analyzing debris evacuation during Ti-6Al-7Nb machining, Journal of Manufacturing Processes 66: 250-268. https://doi.org/10.1016/j.jmapro.2021.04.011.
5. **Wang, Y.; Fan, L.; Shi, J.; Dong, Y.; Fu, Z.** 2023. Effect of cavitation on surface formation mechanism of ultrasonic vibration-assisted EDM, The International Journal of Advanced Manufacturing Technology 124: 3645-3656. https://doi.org/10.1007/s00170-022-10780-5.
6. **Li, Z.; Tang, J.; Bai, J.** 2020. A novel micro-EDM method to improve microhole machining performances using ultrasonic circular vibration (UCV) electrode, International Journal of Mechanical Sciences 175: 105574. https://doi.org/10.1016/j.ijmecsci.2020.105574.
7. **Gao, X.; Li, J.; Xing, Q.; Zhang, Q.** 2022. Research on ultrasonic vibration–assisted electrical discharge machining SiCp/Al composite, The International Journal of Advanced Manufacturing Technology 121(3-4): 2095-2113. https://doi.org/10.1007/s00170-022-09352-4.
8. **Xu, J.; Xia, S.; Yu, P.; Li, M.** 2024. Multi-objective parameter optimization of ultrasonic vibration–assisted micro-EDM of Ti-6Al-4V alloys, Journal of Vibration and Control 30(7-8): 1818-1828. https://doi.org/10.1177/10775463231171798.
9. **Dinh, V. T.; Le, T. Q.; Do, T. T.; Vu, N. P.; Tran, T. P. T.** 2025. Single-Optimization of Ultrasonic Vibration-Assisted EDM for External Cylindrical Machining of 90CrSi, Engineering, Technology & Applied Science Research 15(4): 25959-25970. https://doi.org/10.48084/etasr.11450.
10. **Jatti, V. S.; Khedkar, N. K.; Jatti, A. V.; Jatti, V. S.** 2023. Finite element simulation of electric discharge machining process during machining of NiTi, NiCu and BeCu alloys, Materials Today: Proceedings. https://doi.org/10.1016/j.matpr.2023.01.269.
11. **Arif, U.; Khan, I. A.; Hasan, F.** 2024. Investigating the effect of tool material on performance parameters in electric discharge machining through FEM, Mechanics of Advanced Materials and Structures 31(23): 5906-5914. https://doi.org/10.1080/15376494.2023.2222295.
12. **Papazoglou, E. L.; Karmiris-Obratański, P.; Leszczyńska-Madej, B.; Markopoulos, A. P.** 2021. A study on Electrical Discharge Machining of Titanium Grade2 with experimental and theoretical analysis, Scientific Reports 11(1): 8971. https://doi.org/10.1038/s41598-021-88534-8.
13. **Sharma, A.; Kumar, V.; Babbar, A.; Dhawan, V.; Kotecha, K.; Prakash, C.** 2021. Experimental Investigation and Optimization of Electric Discharge Machining Process Parameters Using Grey-Fuzzy-Based Hybrid Techniques, Materials 14(19): 5820. https://doi.org/10.3390/ma14195820.
14. **Li, M.; Yang, Z.; Dong, H.; Zhou, Y.; Liu, Y.** 2020. Machining performance of high energy die-sinking electrical discharge machining on GH2132, Materials and Manufacturing Processes 35(9): 1024-1031. https://doi.org/10.1080/10426914.2020.1758328.
15. **Sidhu, S. S.; Ablyaz, T. R.; Bains, P. S.; Muratov, K. R.; Shlykov, E. S.; Shiryaev, V. V.** 2021. Parametric Optimization of Electric Discharge Machining of Metal Matrix Composites Using Analytic Hierarchy Process, Micromachines 12(11): 1289. https://doi.org/10.3390/mi12111289.
16. **Perumal, A.; Azhagurajan, A.; Prithivirajan, R.; Kumar, S. S.** 2021. Experimental Investigation and Optimization of Process Parameters in Ti – (6242) Alpha–Beta Alloy Using Electrical Discharge Machining, Journal of Inorganic and Organometallic Polymers and Materials 31(4): 1787-1800. https://doi.org/10.1007/s10904-020-01786-1.
17. **Pratap, P.; Kumar, J.; Verma, R. K.** 2020. Experimental investigation and optimization of process parameters during electric discharge machining of Inconel X-750, Multiscale and Multidisciplinary Modeling, Experiments and Design 3(3): 161-171. https://doi.org/10.1007/s41939-020-00069-z.
18. **Quarto, M; D'Urso, G; Giardini, C.** 2022. Micro-EDM optimization through particle swarm algorithm and artificial neural network, Precision Engineering 73: 63-70. https://doi.org/10.1016/j.precisioneng.2021.08.018.

19. **Ishfaq, K.; Sana, M.; Waseem, M. U.; Ashraf, W. M.; Anwar, S.; Krzywanski, J.** 2023. Enhancing EDM Machining Precision through Deep Cryogenically Treated Electrodes and ANN Modelling Approach, Micromachines 14(8): 1536. https://doi.org/10.3390/mi14081536.
20. **Oniszczuk-Świercz, D; Świercz, R.; Michna, Š.** 2022. Evaluation of Prediction Models of the Microwire EDM Process of Inconel 718 Using ANN and RSM Methods, Materials 15(23): 8317. https://doi.org/10.3390/ma15238317.
21. **Paturi, U. M. R.; Cheruku, S.; Pasunuri, V. P. K.; Salike, S.; Reddy, N. S.; Cheruku, S.** 2021. Machine learning and statistical approach in modeling and optimization of surface roughness in wire electrical discharge machining, Machine Learning with Applications 6: 100099. https://doi.org/10.1016/j.mlwa.2021.100099.
22. **Akar, S; Seyedzavvar, M; Boğa, C.** 2023. A study on the μwire-EDM of $Ni_{55.8}Ti$ shape memory superalloy: an experimental investigation and a hybrid ANN/PSO approach for optimization, Journal of the Brazilian Society of Mechanical Sciences and Engineering 45(3): 171. https://doi.org/10.1007/s40430-023-04100-5.
23. **Dilip, D. G.; Panda, S.; Mathew, J.** 2020. Characterization and parametric optimization of micro-hole surfaces in micro-EDM drilling on Inconel 718 superalloy using genetic algorithm, Arabian Journal for Science and Engineering 45(7): 5057-5074. https://doi.org/10.1007/s13369-019-04325-4.
24. **Dutta, S.; Sarma, D. K.** 2022. Multi-objective optimization of μ-EDM parameters for μ-hole drilling on Hastelloy C 276 super alloy using response surface methodology and multi-objective genetic algorithm, CIRP Journal of Manufacturing Science and Technology 39: 115-133. https://doi.org/10.1016/j.cirpj.2022.07.011.
25. **Zhang, X.; Li, Y.; Yu, P.; Gao, Y.; Dong, S.** 2025. Prediction of microgroove performance indicators based on BP neural network in micro-EDM, Materials Today Communications 46: 112465. https://doi.org/10.1016/j.mtcomm.2025.112465.
26. **Danish, M.; Al-Amin, M.; Rubaiee, S.; Abdul-Rani, A. M.; Zohura, F. T.; Ahmed, A.; Ahmed, R.; Yildirim, M. B.** 2022. Enhanced machining features and multi-objective optimization of CNT mixed-EDM process for processing 316L steel, The International Journal of Advanced Manufacturing Technology 120(9-10): 6125-6141. https://doi.org/10.1007/s00170-022-09157-5.
27. **Lian, H.; Deng, C.; Zhang, L.; Mo, Y.; He, J.; Guo, Z.** 2023. Fabrication of microchannels through template-based electrophoretically assisted micro-ultrasonic machining, The International Journal of Advanced Manufacturing Technology 129(11-12): 5287-5302. https://doi.org/10.1007/s00170-023-12605-5.
28. **Eshaghzadeh, A.; Hajian, A.** 2021. 2-D gravity inverse modelling of anticlinal structure using improved particle swarm optimization (IPSO), Arabian Journal of Geosciences 14(14): 1378. https://doi.org/10.1007/s12517-021-07798-6.
29. **Hu, J.** 2021. Improved Particle Swarm Optimization Integrating Multiple Strategies, Computer Systems Applications 30: 172-177. https://doi.org/10.15888/j.cnki.csa.007989.
30. **Mo, D.; Bai, L.; Huang, W.; Wu, N.; Lu, L.** 2024. TBM disc cutter wear prediction using stratal slicing and IPSO-LSTM in mixed weathered granite stratum, Tunnelling and Underground Space Technology 148: 105745. https://doi.org/10.1016/j.tust.2024.105745.

L. Chen, H. Lian, Y. Ling, S. You, D. Mo, L. Zhang, G. Wang

PROCESS OPTIMIZATION OF ULTRASONIC VIBRATION-ASSISTED ELECTRICAL DISCHARGE MACHINING FOR BRASS NOZZLES BASED ON ORTHOGONAL EXPERIMENTS AND IPSO-BP MODEL

S u m m a r y

Ultrasonic vibration assisted electrical discharge machining (EDM) is a novel precision machining method capable of further enhancing the efficiency and quality of EDM. Brass is frequently utilized as the material for precision agricultural spray nozzles due to its corrosion resistance and superior wear resistance compared to plastics. To obtain the optimal process parameters for ultrasonic vibration assisted EDM of brass, an orthogonal experiment scheme with five factors and four levels was designed. The material removal rate (MRR) and electrode wear rate (EWR) were selected as the primary evaluation indicators, while machining voltage, spindle speed, ultrasonic power, pulse frequency, and feed rate served as the main process parameters. Simultaneously, an improve particle swarm optimization (IPSO)-BP neural network model is train based on the results of the orthogonal experiments. By combining the aforementioned methods, the optimal process parameters for MRR were determined as follows: machining voltage of 95V, spindle speed of 2000 r/min, ultrasonic power of 45%, pulse frequency of 25 kHz, and electrode feed rate of 0.20 mm/s. The optimal process parameters for EWR were identified as: machining voltage of 65V, spindle speed of 3000 r/min, ultrasonic power of 75%, pulse frequency of 30 kHz, and feed rate of 0.16 mm/s. In the verification of above two sets of optimal parameters, the IPSO-BP model achieved R^2 accuracies of 87% and 94%, respectively. The overall prediction performance of the model is satisfactory, indicating that the model is capable of assisting and guiding the formulation of process plans for the subsequent ultrasonic vibration assisted EDM of brass nozzles.

Keywords: EDM, ultrasonic vibration assisted, orthogonal experiments, IPSO-BP neural network, process optimization.

Received March 3, 2026
Accepted June 19, 2026